

Geol. Jb.	D 92	231 — 253	5 Fig.	5 Tab.	Hannover 1990
-----------	------	-----------	--------	--------	---------------

Stable Isotope Stratigraphy, Paleo productivity and Sedimentation Rates in the South Lau and North Fiji Basins, Southwest Pacific Ocean

KYAW WINN, MICHAEL WIEDICKE & HELMUT ERLKENKEUSER

Cruise (SONNE, SO-35), sediment cores, stable isotope stratigraphy, ^{18}O , total carbonate, ^{13}C , foraminifers (*Globigerinoides ruber*, *Cibicidoides wuellerstorfi*), paleoproductivity, sedimentation rates, biomass, dating, volcanic ashes

Southwest Pacific, North Fiji Basin, Lau Basin

Abstract: Stable isotope measurements on the planktonic foraminifer *Globigerinoides ruber* (*white*) have been carried out on a number of selected deep-sea sediment cores from the South Lau and North Fiji Basins. The $\delta^{18}\text{O}$ -curves show good correlation with the inter-ocean graphic correlation composite $\delta^{18}\text{O}$ -record of the standard reference section (PRELL et al. 1986), which, in combination with the chronostratigraphic classifications of HERTERICH & SARNTHEIN (1984, modified) and IMBRIE et al. (1984), allow a detailed dating of the sedimentary sequences. The deepest layers in core no. 119 (southern Lau Basin) could be assigned to Isotope Stage 24. Measurements made on bulk carbonate in two cores show a much higher glacial-interglacial amplitude, allowing the general identification of the conventional oxygen isotope stages.

The $\delta^{13}\text{C}$ -values of the benthic foraminifer *Cibicidoides wuellerstorfi* show progressively lighter values northwards reflecting an increasing contribution of the isotopically lighter CO_2 from the remineralisation of organic matter during the general northward movement of the deep water masses.

Cyclicities in the sedimentation rates were observed in core nos. 117 and 119 (both southern Lau Basin) where the interglacials exhibit higher levels than the glacials. Calculated new or export paleoproductivity show that the glacials had higher productivity in the euphotic zone.

From the oxygen isotope stratigraphy, the five ash layers in core nos. 117 and 119 could be dated as about 530 ka B.P. in Stage 14, 695 ka B.P. in Stage 18, 775 ka B.P. in Stage 21, 790 ka B.P. and 825 ka B.P. in Stage 22. Carbonate dissolution occurred during stages 5, 8 and 10 to 12.

[Stratigraphie der stabilen Isotope, Paläoproduktivität und Sedimentationsraten im Süd-Lau-Becken und im Nord-Fidschi-Becken, Südwest-Pazifik]

Für eine Auswahl von Tiefseekernen, die 1985 auf der Forschungsfahrt SO-35 von F.S. SONNE in dem südlichen Lau-Becken und dem nördlichen Fidschi-Becken gewonnen wurden, wurden die Foraminiferen-Isotopenstratigraphien erstellt.

Die $\delta^{18}\text{O}$ -Profile zeigen eine gute Korrelation mit dem verallgemeinerten ozeanübergreifenden graphischen Korrelations- $\delta^{18}\text{O}$ -Profil von PRELL et al. (1986) und erlauben in Verbindung mit den modifizierten CARTUNE- und SPECMAP-Zeitskalen (HERTERICH & SARNTHEIN 1984; IMBRIE et al. 1984) eine ins Einzelne gehende zeitliche Einstufung.

Die tiefsten Lagen in Kern 119 (südliches Lau-Becken) gehören zum Isotopenstadium 24 (ca. 900 ka B.P.). Die Kerne weisen keine größeren Schichtlücken auf; ihre Sedimentationsraten betragen im Lau-Becken 1 bis 2 cm/1000 a (ohne Aschenlagen) und bis zu 6 cm/1000 a in Turbidit-haltigen Sequenzen im Fidschi-Becken. Periodische Wechsel der Sedimentationsrate waren nicht fest-

Authors' addresses: Dr. KYAW WINN, Geologisch-Paläontologisches Institut, Christian-Albrechts-Universität, Ludewig Meynstr. 10, D-2300 Kiel. Dr. M. WIEDICKE, Bundesanstalt für Geowissenschaften und Rohstoffe, Stilleweg 2, D-3000 Hannover 51. Dr. H. ERLKENKEUSER, Institut für Reine und Angewandte Kernphysik, C14-Labor, Christian-Albrechts-Universität, Leibnizstr. 19, D-2300 Kiel.

zustellen, mit Ausnahme der Kerne 117 und 119, in denen die Interglaziale höhere Akkumulationsraten als die Glaziale zeigen.

Die Kerne im Lau-Becken zeigen eine Reihe von Aschenlagen. Die Alter der 5 mächtigeren vulkanogenen Glassilte in den Kernen 117 und 119 liegen bei etwa 530 ka B.P. in Isotopenstadium 14, bei 695 ka B.P. in Stadium 18, bei 775 ka B.P. in Stadium 21 sowie bei 790 ka und 825 ka in Stadium 22. Die 530 ka alte Aschenlage mißt in Kern 110 ca. 2 m. Starke Karbonatlösung trat in den Stadien 5, 8 sowie 10 bis 12 auf.

Isotopenanalysen am Gesamtkarbonat ($> 160 \mu\text{m}$) der Kerne 110 (Lau-Becken) und 180 (Nord-Fidschi-Becken) zeigen im großen und ganzen ebenfalls die typische Abfolge der Isotopenstadien. Allerdings sind die glazial-interglazialen Amplituden des $\delta^{18}\text{O}$ -Signals gegenüber der Isotopenstratigraphie an einer einzelnen Foraminiferenart durch selektive Lösung vergrößert.

Die $\delta^{13}\text{C}$ -Werte der benthischen Foraminifere *Cibicidoides wuellerstorfi* werden mit nördlicherer Kernposition zunehmend leichter, sowohl in den Glazial- wie in den Interglazialstadien. Diese isotopische Verschiebung resultiert aus dem mit der Laufzeit des Tiefenwassers ansteigenden Beitrag von isotopisch leichtem CO_2 aus der Remineralisation organischer Substanz. Insofern stehen die $\delta^{13}\text{C}$ -Ergebnisse im Einklang mit der allgemeinen nordwärts gerichteten Ausbreitung des Tiefenwassers im SW-Pazifik.

Die aus den Sedimentdaten errechneten Paläo-Neuproduktivitäten ergeben eine höhere Produktivität der euphotischen Zone während der Glazialstadien.

Contents

	Page
1 Introduction	233
2 Methods	234
3 Stable Isotope Stratigraphy	234
3.1 Planktonic Foraminifera	234
3.2 Benthic Foraminifera	240
3.3 Bulk Carbonate	240
4 Paleoproductivity	242
5 Conclusions	242
6 References	243
Appendix: Tables 1—5	245

1 Introduction

From the large number of deep-sea sediment cores taken in 1985 during cruise no. 35 of the RV SONNE (VON STACKELBERG et al., this volume), core nos. 101, 117 and 119 from the South Lau Basin and core no. 272 from the North Fiji Basin were selected for species-specific stable isotope (oxygen and carbon) investigations. In addition, the upper sections of core no. 182, the pilot cores of nos. 102 (South Lau Basin) and 211 (North Fiji Basin) were analysed (Fig. 1, Table 1)*).

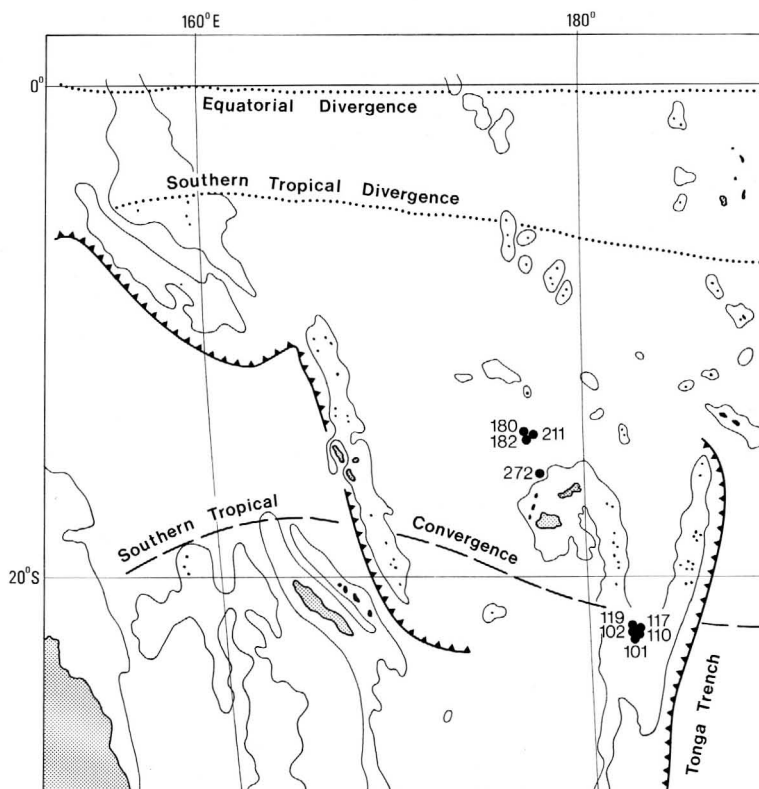


Fig. 1: Map showing location of the analysed cores. All cores have the prefix SO 35- .
2000 fathoms depth is contoured.

Stable isotope measurements on the bulk carbonate of core nos. 110 and 180 were also made. All these cores were located in the deeper parts of the basins, and the studied pelagic sections exhibit lesser disturbances through slumps, turbidites and large volcanic debris, compared to most of the other cores (RIECH, this volume).

*) For Tables 1–5 see Appendix

2 Methods

The upper meter of sediment in all the cores was sampled at very close intervals (1–2 cm) for measurement of physical and chemical properties such as dry and wet bulk densities, water, carbonate and organic carbon contents (as weight %). Down the core, the sample intervals were increased to 4 cm in core no. 272, and generally to 10–15 cm in the other cores. In core nos. 101 and 110, sampling was stopped at the thick ash layer present around 9 m sediment depth in both cores. Plastic syringes (5 and 10 ml) were generally used in sampling. About 1 ml of sediment was expended for carbonate and organic carbon measurements, which were performed at the Geological-Palaeontological Institute in Kiel, using both the LECO CS-244 and COULOMAT 701 instruments. The sulphur content was obtained additionally during the course of the measurements with the LECO instrument. Vacuum drying of samples of known volume and weight for calculating the water content and sediment density, ensured that the samples remained fluffy and suitable for further investigations. Wet sieving to wash out the clay-silt fraction was carried out both at Kiel, and at the Federal Geological Survey in Hannover.

For stable isotope studies, about 10 to 20 specimens of the planktonic foraminifer *Globigerinoides ruber* (white), and the available tests of the benthic *Cibicidoides wuellerstorfi* were picked, mainly from the 315–400 μm grain size fraction. *G. conglobatus* was chosen at intervals where *G. ruber* was absent or occurred sporadically. In core 101, the < 315 μm fraction of *G. ruber* was also picked. The specimens were cleaned with methanol in a sonic bath for about fifteen seconds. The measurements were made with a Finnigan MAT 251 mass spectrometer at the ^{14}C -Laboratory of the Institute of Pure and Applied Nuclear Physics, Kiel. This instrument is on-line fitted to the CARBO KIEL device for automated CO_2 preparation from carbonate samples (down to 10 μg) for isotope analysis. The system can routinely measure with an accuracy — on the δ -scale — of $\pm 0.07\text{‰}$ for oxygen and $\pm 0.04\text{‰}$ for carbon isotopes, respectively. The results were reported on the PDB scale (international isotope reference scale, based on a belemnite carbonate aliquot *Belemnitella americana* from the Peedee Formation of South Carolina).

For core nos. 110 and 180, bulk carbonate of the > 160 μm fraction was used for analysis. The samples were lightly crushed, cleaned ultrasonically, and analysed on the VG 602 mass spectrometer at the Federal Geological Survey (BGR) laboratories in Hannover.

3 Stable Isotope Stratigraphy

3.1 Planktonic Foraminifera

In assigning oxygen isotope events and their ages, we have used the modified CARTUNE time scale of HERTERICH & SARNTHEIN (1984). This scale also compensates for the effects of carbonate dissolution, but has significant differences to the spectral time scale of IMBRIE et al. (1984), especially in the older sections below Stage 12. Part of this discrepancy might result from stratigraphic disturbances due to possible nondepositional, dissolution, or erosional episodes (hiatus) which could easily remain unrecognized in a long geologic section when only one core was used, and to the known technical problems of compression and extension during the coring procedure. In order to surmount these difficulties, our oxygen isotope stage boundaries followed the graphic correlation composite $\delta^{18}\text{O}$ -record of the standard reference section (PRELL et al. 1986) for the Brunhes Chron. This profile was based on the stacked records of 13 cores. The corresponding ages from the modified CARTUNE time scale were then assigned to these stage boundaries up to Stage 12. Below this stage, the SPECMAP chronology of IMBRIE et al. (1984) was applied.

The oxygen isotope stratigraphy is supported by the following three well known and widely used datums:

- i — the disappearance of the pink-pigmented planktonic foraminifer *G. ruber* in the Pacific at around 120 ka B.P. in Stage 5e (THOMPSON et al. 1979).
- ii — the extinction of the coccolith *Pseudoemiliania lacunosa* within Stage 12 at about 450 ka B.P. (THIERSTEIN et al. 1977).
- iii — the paleomagnetic Brunhes/Matuyama boundary at the beginning of Stage 19 at around 730 ka B.P. (MANKINEN & DALRYMPLE 1979).

The depths of the first two events in the investigated cores have been determined by RIECH (this volume), and of the third by VON DOBENEK & PETERSEN, Institute of General and Applied Geophysics, University of Munich.

Linear regression analysis of the stable isotope data of the 315–400 μm and 250–315 μm fractions of *G. ruber* in core no. 101 was made with the simple linear model,

$$y = a + bx,$$

where a and b are constants, and y and x are the isotope values of the 315–400 μm and 250–315 μm size fractions, respectively. The analysis of 44 $\delta^{18}\text{O}$ -data pairs, with the root mean square deviation of the points measured perpendicular to the regression line, yields the results

$$a = -0.02 \pm 0.03 \text{ ‰} \quad \text{and} \quad b = 0.91 \pm 0.04,$$

with a correlation coefficient of 0.80. The deviations from a 1:1 relationship are minimal and lie within the range of the instrument accuracy (Fig. 2a). Therefore, the $\delta^{18}\text{O}$ -values of the 250–315 μm size fraction have been included in drawing the composite isotope record of this core. The stable isotope values for core nos. 101, 117 and 119, and 272 are given in Table 2 a to d.

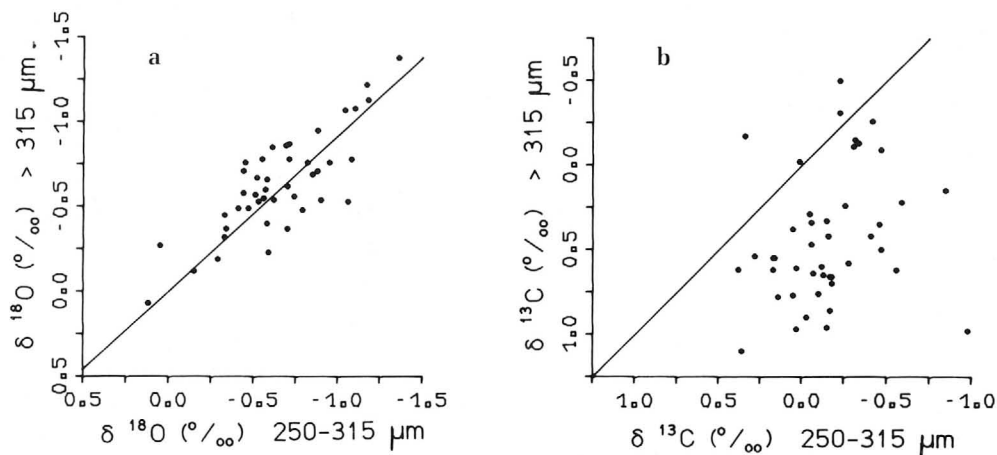


Fig. 2: Plots showing the relationship between the

(a) $\delta^{18}\text{O}$ -values and

(b) $\delta^{13}\text{C}$ -values of the 250–315 μm and 315–400 μm size fractions of *G. ruber* in core SO 35-101.

The regression line in (a) represents $\delta^{18}\text{O}$ (315–400 μm) = $0.91 * \delta^{18}\text{O}$ (250–315 μm) - 0.02 while in (b), the 45°-line is shown.

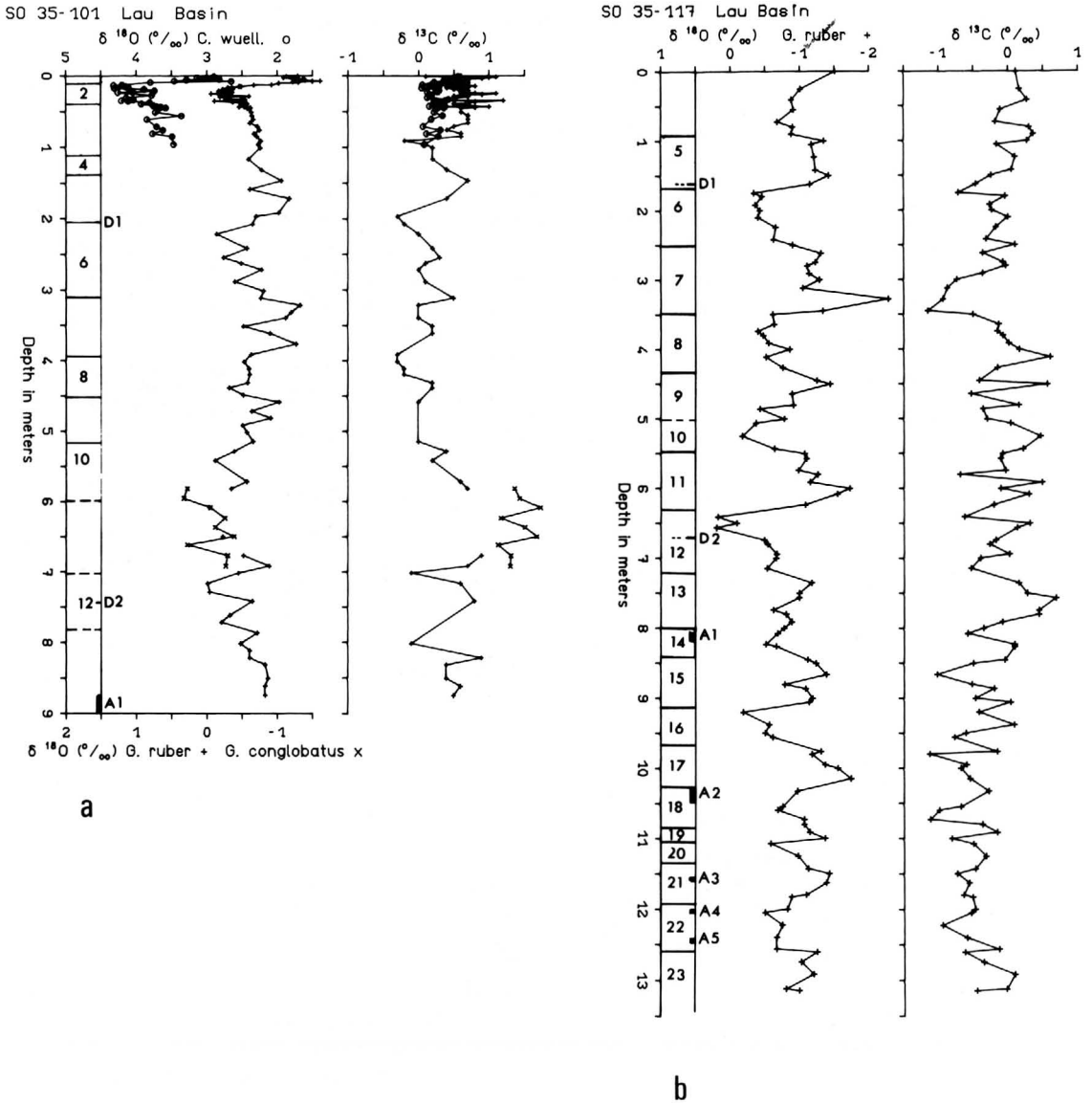
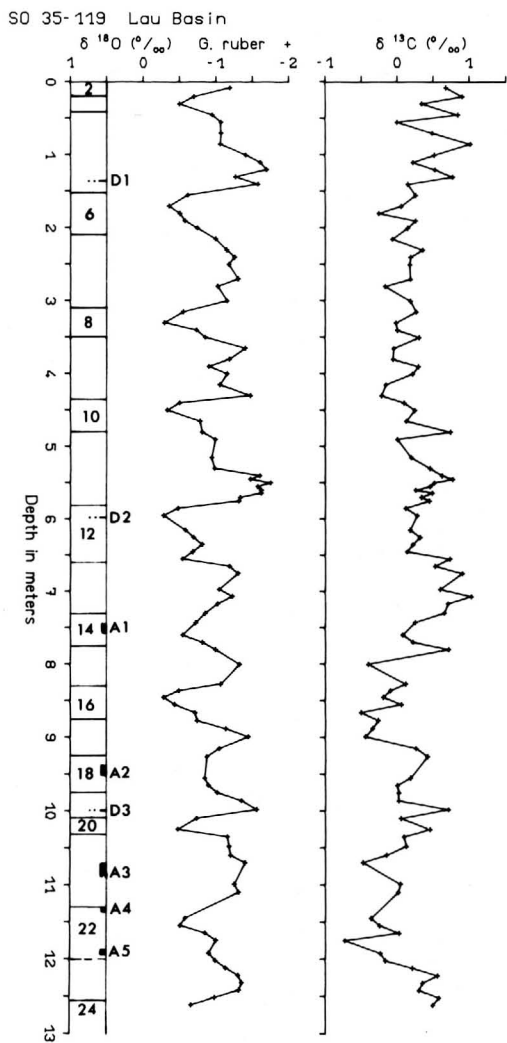
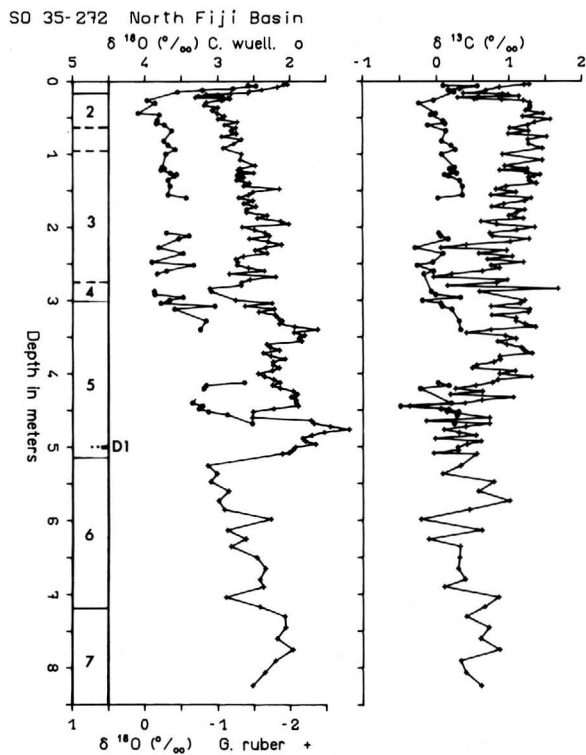


Fig. 3: Stable isotope records of cores SO 35-101 (a), SO 35-117 (b), SO 35-119 (c), and SO 35-272 (d). A1 to A5 mark the positions of the ash layers, D1 = *G. ruber* (pink) disappearance at 120 ka B.P., D2 = *P. lacunosa* extinction level at about 450 ka B.P., and D3 = the Brunhes-Matuyama paleomagnetic boundary at about 730 ka B.P.



c



d

A significant relationship could not be defined for the carbon isotopes of the two size fractions, probably because of the smaller range in the values between the size fractions coupled with a higher natural variability. Nevertheless, Figure 2 (b) shows that the smaller specimens are generally lighter by about 0.7 ‰ than the larger tests. DUPLESSY et al. (1975), BERGER et al. (1978), and DUNBAR & WEFER (1984) found similar interspecific, as well as size-dependent variations in $\delta^{13}\text{C}$. These findings emphasize the need for selecting a well defined size fraction from the total calcareous assemblage, for species-specific isotopic analysis. Therefore, only the carbon isotope values of the 315-400 μm size fraction are shown in Figure 3a.

Although the cores have been selected for their apparently continuous pelagic sediment records, the effects of slumps and volcanic debris are noticeable. The $\delta^{18}\text{O}$ -values of the glacial stages in the cores from the South Lau Basin, for instance, are not as pronounced as in the graphic composite of PRELL et al. (1986), probably due to the presence of allochthonous tests in the samples. An example is the very light value exhibited by *G. ruber* in the lower part of Stage 7 in core no. 117. Furthermore, there are significant inter-core differences in the oxygen isotope levels of the same species which are much higher than expected for such local basins (Table 2 a to d). These phenomena may have resulted from reworking and lateral transport. In spite of these limitations, the oxygen isotope stratigraphies given by *G. ruber* show that the glacial and interglacial stages are well documented in the core sections studied here (Fig. 3 a to d) with a glacial-interglacial amplitude of about 1.2 ‰ to 1.6 ‰. The stages mainly reflect, isotopically, the global ice volume effects that have been reported, for instance, from the deep-sea sediment sequences of the eastern Pacific (SHACKLETON & OPDYKE 1973), and from the eastern equatorial Atlantic (SARNTHEIN et al. 1984).

The ages of the oxygen isotope stage boundaries and their depths in the cores, as well as the average sedimentation rates are given in Table 3. For core no. 101 (Fig. 3a), there is also a generally good agreement with the sedimentation rates calculated from the Th-230 profile measured down to 4 m (MANGINI & STOFFERS, this volume). Pronounced cyclicities in the sedimentation rates are not observed, probably due to the ubiquitous pumice and downslope transport. Exceptions are core nos. 117 and 119 from the Lau Basin which penetrated down to the top of Stage 24. The five major ash layers A1 to A5 (Fig. 3b and c) encountered below 7.5 m in these cores were deposited during stages 14 (530 ka B.P.), 18 (695 ka B.P.), 21 (775 ka B.P.) and 22 (790 ka B.P. and 825 ka B.P.), respectively. Taking into account the anomalously higher sedimentation rates due to this ash input, a strong cyclicity is observed below Stage 5, with the interglacials exhibiting the higher rates. The isotopic values of *G. ruber* remain almost on the same level for the glacial stages 6 to 16. Lighter values prevailed during the Last Glacial, Stage 14, and in glacial Stage 18 and older. These trends are similar to those shown by the oxygen isotope curve of *Globigerinoides sacculifera* in core V28-238 (SHACKLETON & OPDYKE 1973) further north, with the exception that Stage 20 already exhibited the heavier value. However, this may be a question of resolution, which is dependent upon the sampling intervals.

In the sediment section between 5.8 m to 6.7 m (isotope stages 10 and 11) in core no. 101, the stage boundaries are tentative because of the gap in the *G. ruber* curve (non-preservation) which could not safely be complemented by the *G. conglobatus* isotopic values. The abnormally high sedimentation rates during Stages 10 and 11 are not an artifact resulting from the uncertainty of the positions of the stage boundaries. It could neither be explained through increased volcanic activity nor higher carbonate production, since the thinner shelled *G. ruber* were selectively dissolved in this core section.

In core no. 272 (Fig. 3d), our lowest studied horizon could be assigned to Stage 7. The high sedimentation rates in core 272 coupled with the narrow spaced sampling interval resulted in a high resolution isotope stratigraphy. The much lighter level of the younger 5e peak compared to the Holocene, may be due to allochthonous influence. The boundary between stages 2 and 3 after *G. ruber* lies much lower than that after *C. wuellerstorfi* (Figs. 3d and 4).

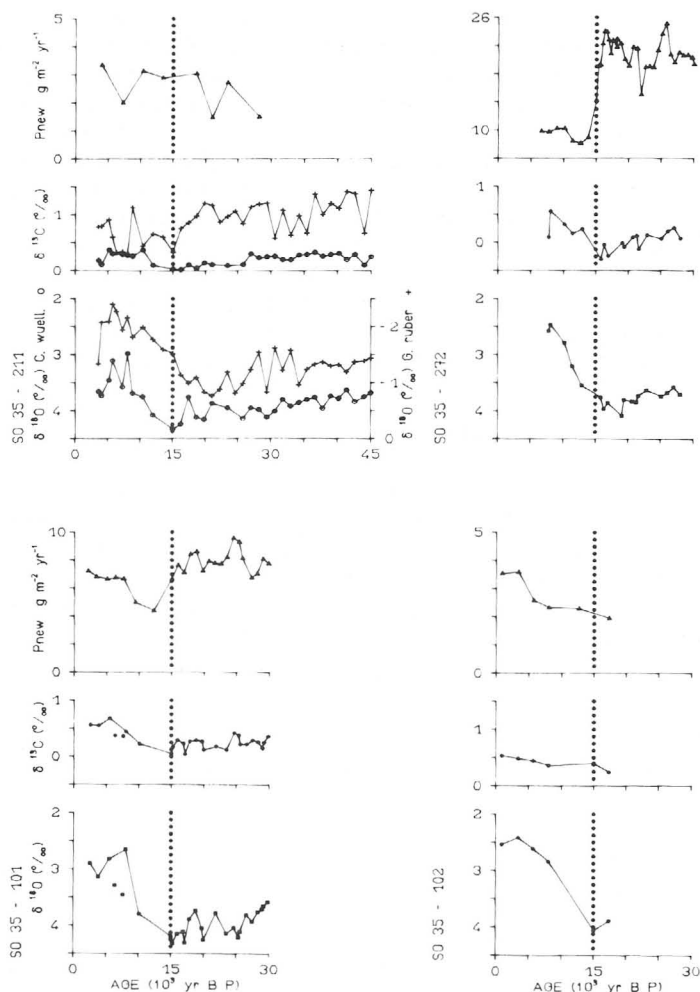


Fig. 4: Stable isotope records of *C. wuellerstorfi* (SO 35-211 also with *G. ruber*), and paleoproductivity (new) records of the cores SO 35-101, SO 35-102, SO 35-211 and SO 35-272 for the past 30,000 years. *C. kullenbergi* values in SO 35-101 not joined.

3.2 Benthic Foraminifera

The benthic foraminifer *C. wuellerstorfi* was additionally analysed in the uppermost part of the cores, so that both planktonic and benthic isotope curves are available for detailed stratigraphic analysis. The high resolution isotope records resulting from the dense sampling (sample interval 1–1.5 cm) show that in all the cores, the true recent surface was missing. Probably, these unconsolidated sediments were lost due to the coring technique. The detailed isotopic characteristics were used to establish the time frame (stratigraphy after SARNTHEIN et al. 1988), in order to show the downcore isotope distribution along with the paleoproductivity on a time scale (Fig. 4). Core 182 was not shown since the Holocene values were missing in the oxygen isotope data.

The $\delta^{13}\text{C}$ -values of *C. wuellerstorfi* reflect in part the ocean surface productivity signal (SARNTHEIN et al. 1988) and in part the general aging of the deep sea bottom water masses (DUPLESSY et al. 1984). This response could be attributed to the metabolic activity, e.g. respiration of the benthos, and to the decomposition (remineralisation) of organic matter, the flux of which relates to the net exported primary productivity in the euphotic zone. Our $\delta^{13}\text{C}$ -values from *C. wuellerstorfi* are in accordance with the general northwards movement of the deep water masses, a view which is further corroborated by the results of VINCENT et al. (1981) from the Ontong-Java Plateau farther to the north. The surface productivity effect (see also section on paleoproductivity below) can be clearly observed in the $\delta^{13}\text{C}$ -levels for both the Last Glacial and the Holocene. The values decrease from 0.20 ‰ in core no. 101 to 0.0 ‰ in core no. 272, to - 0.23 ‰ in the ERDC cores (VINCENT et al. 1981) for the Last Glacial. For the generally lower productive Holocene, the $\delta^{13}\text{C}$ changes are much lesser, ranging from 0.56 ‰ in core no. 101 to 0.37 ‰ in core no. 272 (Fig. 4) to 0.30 ‰ in the ERDC cores.

3.3 Bulk Carbonate

Isotopic results on bulk carbonate samples are dependent, among other factors, upon the depth and hence temperature of the habitat, diversity, size distribution and abundance of the different species in the assemblage, since not all species live in isotopic equilibrium with the seawater. Species-selective dissolution events and diagenetic processes may further alter the isotope composition of the sediment column.

The measurements on core nos. 110 (Lau Basin) and 180 (North Fiji Basin) yield a much larger difference (2 ‰ to 2.5 ‰) between the heavier glacial values and the lighter interglacial levels (Fig. 5) than is shown by the monospecific isotope curves. However, the results do allow the general identification of the major climatic cycles. A fairly good fit is also observed with the *P. lacunosa* extinction level and the *G. ruber* (pink) disappearance datum mentioned previously. Detailed sedimentation rates have not been calculated since the stage boundaries could not be safely placed.

The large amplitude of the bulk carbonate $\delta^{18}\text{O}$ -curve in core no. 110 (Fig. 5) has been interpreted as resulting from selective dissolution of the thin-shelled planktonic foraminifera, which led to a relative enrichment of the isotopically "heavier" components such as *G. conglobatus* and benthic species. The interval between 3.5 m and 7.5 m indicates a general trend towards heavier isotope values thought to be generated by selective dissolution.

Microscopic examination of the samples which gave even stronger deviations (Table 4) confirm that they were composed of extremely corroded foraminiferal assemb-

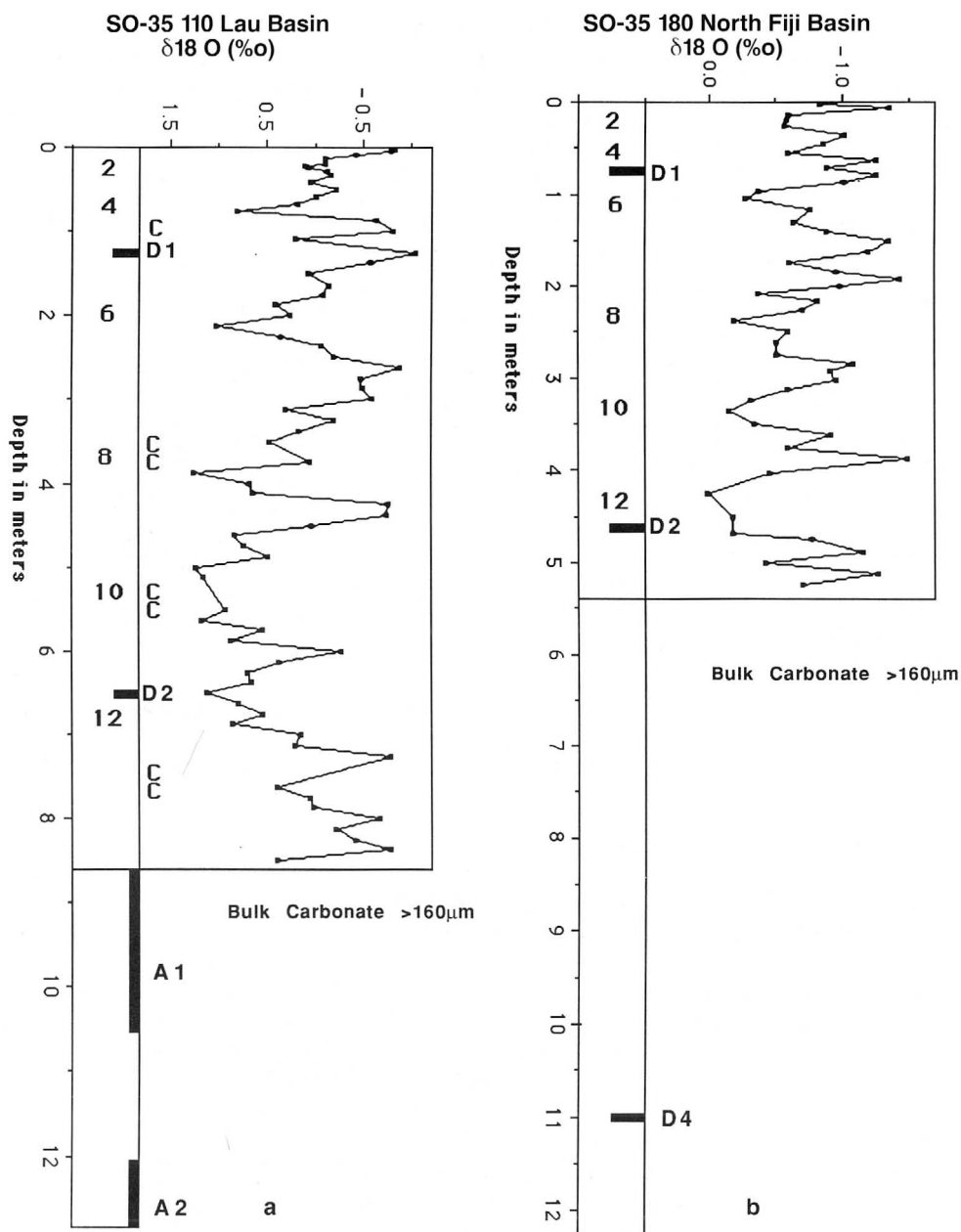


Fig. 5: Oxygen isotope records measured on bulk carbonate of cores SO 35-110 (a), Lau Basin and SO 35-180 (b), North Fiji Basin.

A1 to A2 mark the positions of ash layers,

D1 = *G. ruber* (pink) disappearance at 120 ka B.P.,

D2 = *P. lacunosa* extinction level at about 450 ka B.P.,

D4 = Disappearance of discoasterids, Tertiary/Quaternary boundary,

C = Strongly corroded foram assemblages (see Table 5).

lages, where thin-shelled tests were absent and probably have suffered from dissolution. The 'C'-labelled depths in the corelog mark the position of these corroded horizons where the residual assemblage consisted mainly of globorotaliids and thick-walled (*G. conglobatus*) specimens.

4 Paleoproductivity

The upper parts of the cores were studied in detail for paleoproductivity changes through the last glacial to the present. The paleoproductivity (new or export productivity) is calculated from empirical relationships (SARNTHEIN et al. 1987, 1988) using the organic carbon content, sedimentation rate and dry bulk density, and also taking into account the water depth of the core. The calculated paleoproductivities from the last glacial up to the present are shown in Figure 4 and listed in Table 5. Because the very low organic carbon contents in two of these cores (nos. 102 and 211) are not always accurately measureable with our available instruments, only the results from core no. 101 (South Lau Basin) and no. 272 (North Fiji Basin) have been used in the interpretation. They show that in the South Lau Basin, the glacial productivity values were generally higher by about 18 % than the Holocene data. This contrast increases to over 100 % in the higher productivity environment of the North Fiji Basin. The geographical position of the cores (Fig. 1) show that core no. 101 is located almost directly under the present day Southern Tropical Convergence Zone while core no. 272 lies about 450 km to the north, halfway to the comparatively fertile Southern Tropical Divergence around 8° S latitude.

The carbonate accumulation rates for the above cores show that the North Fiji Basin had a higher carbonate productivity than the South Lau Basin during the Last Glacial and Holocene. Core no. 101 from the South Lau Basin shows a larger decrease (- 26 %) between the Last Glacial and the Holocene than core nos. 211 and 272 (- 12 %) from the North Fiji Basin.

5 Conclusions

The oxygen isotope stratigraphies of sediment cores from the South Lau and North Fiji basins show continuous sediment records reaching down to about 900 ka B.P with a glacial-interglacial $\delta^{18}\text{O}$ -amplitude of about 1.3 ‰. With the possible exception of small disconformities, large hiatuses have not been identified. The isotope chronology also fits closely with the age of the paleomagnetic Brunhes-Matuyama boundary, the coccolith *P. lacunosa* extinction level and the pink-pigmented *G. ruber* disappearance datum (RIECH, this volume).

Paleoproductivities were generally higher during the Last Glacial than in the Holocene. The $\delta^{13}\text{C}$ -values of the benthic foraminifer *C. wuellerstorfi* clearly show a trend towards lighter levels northwards.

Major eruptive volcanic activity resulting in sizeable ash fallout occurred during oxygen isotope stages 14, 18, 21, and 22 in the South Lau Basin. The last thick ash layer (over 2 m thick in core no. 110) was deposited at about 530 ka B.P.

Heavy corrosion and dissolution of carbonate occurred during oxygen isotope stages 5 and 8, and intermittently during stages 10 to 12. These effects are more pronounced in core no. 110 than in core no. 101.

With the exception of core nos 117 and 119 where the interglacials showed faster sediment deposition, a cyclicity in the accumulation rates could not be substantiated. A general fit with the rates calculated from ^{230}Th profiles (MANGINI & STOFFERS, this volume) is observed.

Acknowledgements: We are grateful to Mr. H. CORDT at the C 14-Laboratory of the Institute of Pure and Applied Nuclear Physics, Kiel, for the maintenance of the mass spectrometer and expert support with/during the measurements, and to Professor M. SARNTHEIN for advice in working out the detailed stratigraphies in the upper sections of the cores. We are also grateful to T. VON DOBENEK and Professor N. PETERSEN, Institute of General and Applied Geophysics, University of Munich, for determination of the paleomagnetic Brunhes-Matuyama boundary in selected cores. This work is funded in part by the National Climate Project of the German Federal Ministry of Research and Technology, grant no. KF 2004/1.

6 References

- BERGER, W. H., KILLINGLEY, J. S., & VINCENT, E. (1978): Stable isotopes in deep-sea carbonates: box core ERDC-92, west equatorial Pacific. — *Oceanol. Acta*, **1**: 203–216.
- DUNBAR, R. B., & WEFER, G. (1984): Stable isotope fractionation in benthic foraminifera from the Peruvian continental margin. — *Mar. Geol.*, **59**: 215–225.
- DUPLESSY, J. C., CHENOUEARD, L., & VILLA, F. (1975): Weyl's theory of glaciation supported by isotopic study of Norwegian core K 11. — *Science*, **188**: 1208–1209.
- , SHACKLETON, N. J., MATTHEWS, R. K., PRELL, W., RUDDIMAN, W. F., CARALP, M., & HENDY, C. H. (1984): ^{13}C -record of benthic foraminifera in the last Interglacial Ocean: Implications for the carbon cycle and the global deep water circulation. — *Quat. Res.*, **21**: 225–243.
- HERTERICH, K., & SARNTHEIN, M. (1984): Brunhes Time Scale: Tuning by rates of calcium-carbonate dissolution and cross spectral analyses with solar insolation. — In: BERGER, A., IMBRIE, J., HAYS, J., KUKLA, G., & SALTZMAN, B. (Eds.): *MILANKOVITCH and Climate, Part I*: 447–466; Dordrecht (Reidel).
- IMBRIE, J., HAYS, J. D., MARTINSON, D. G., MCINTYRE, A., MIX, A. C., MORLEY, J. J., PISIAS, N. G., PRELL, W. L., & SHACKLETON, N. J. (1984): The Orbital Theory of Pleistocene climate: Support from a revised chronology of the marine $\delta^{18}\text{O}$ -record. — In: BERGER, A., IMBRIE, J., HAYS, J., KUKLA, G., & SALTZMAN, B. (Eds.): *MILANKOVITCH and Climate, Part I*: 269–305; Dordrecht (Reidel).
- MANGINI, A., & STOFFERS, P. (1990): A high resolution ^{230}Th depth profile in a piston core from the Southern Lau Basin (Southwest Pacific). — *Geol. Jb.*, **D 92**: 255–261; Hannover. — [This Vol.]
- MANKINEN, E. A., & DALRYMPLE, G. B. (1979): Revised geomagnetic polarity time scale for the interval 0–5 m.y. B.P. — *Jour. Geophys. Res.*, **84/B2**: 615–626.
- PRELL, W. L., IMBRIE, J., MARTINSON, D. G., MORLEY, J. J., PISIAS, N. G., SHACKLETON, N. J., & STREETER, H. F. (1986): Graphic correlation of oxygen isotope stratigraphy application to the late Quaternary. — *Paleoceanography*, **1**, 2: 137–162.
- RIECH, V. (1990): Calcareous oozes, volcanic ashes, and metalliferous sediments in the Quaternary of the Lau and North Fiji Basins. — *Geol. Jb.*, **D 92**: 109–162; Hannover. — [This Vol.]
- SARNTHEIN, M., ERLKENKUSER, H., GRAFENSTEIN, R. VON, & SCHROEDER, C. (1984): Stable isotope stratigraphy for the last 750,000 years: "Meteor" core 13519 from the eastern equatorial Atlantic. — "Meteor" *Forsch. Ergbn.*, **C 38**: 9–24.
- , WINN, K., DUPLESSY, J. C., & FONTUGNE, M. R. (1988): Global variations of surface ocean productivity in low and mid-latitudes: Influence on CO_2 reservoirs of the deep ocean and atmosphere during the last 21,000 years. — *Paleoceanography* **3**: 361–399.

- , —, & ZAHN R. (1987): Paleoproductivity of oceanic upwelling and the effect of atmospheric CO₂ and climatic change during deglaciation times. — In: BERGER, W. H., & LABEYRIE, L. D. (Eds.): *Abrupt Climatic Change*: 311–337; Dordrecht (Reidel).
- SHACKLETON, N. J., & OPDYKE, N. D. (1973): Oxygen-isotope and paleomagnetic stratigraphy of Pacific core V28–238: Oxygen isotope temperatures and ice volumes on a 10⁵ year and 10⁶ year scale. — *Quat. Res.*, **3**: 39–55.
- STACKELBERG, U. VON, RAD, U. VON, & RIECH, V. (1990): SONNE cruise SO-35 in the Lau and North Fiji Basins (SW Pacific Ocean). — *Geol. Jb.*, **D 92**: 7–36; Hannover. — [This Vol.]
- THIERSTEIN, H. R., GEITZENAUER, K. R., MOLFINO, B., & SHACKLETON, N. J. (1977): Global synchronicity of late Quaternary coccolith datum levels: Validation by oxygen isotopes. — *Geology*, **5**: 400–404.
- THOMPSON, P. R., BE, A. W. H., DUPLESSY, J.-C., & SHACKLETON, N. J. (1979): Disappearance of pink-pigmented *Globigerinoides ruber* at 120,000 B.P. in the Indian and Pacific Oceans. — *Nature*, **280**: 554–558.
- VINCENT, E., KILLINGLEY, J. S., & BERGER, W. H. (1981): Stable isotopes in benthic foraminifera from Ontong-Java Plateau, Box cores ERDC 112 and 123. — *Palaeogeogr., Palaeoclimatol., Palaeoecol.*, **33**: 221–230.

Appendix

Tables 1–5

Table 1. Locations of the analysed cores

Core no.	Sediment Basin	Latitude	Longitude	Depth b.s.l.	Remarks
SO35-101	South Lau	22°26.9'S	177°19.8'W	3125 m	analysed to 8.75 m
SO35-102	South Lau	22°24.3'S	177°26.9'W	2910 m	pilot core, to 0.33 m
SO35-110	South Lau	22°15.8'S	177°20.6'W	2970 m	analysed to 8.50 m
SO35-117	South Lau	22°08.4'S	177°21.7'W	2670 m	analysed to 13.16 m
SO35-119	South Lau	22°00.5'S	177°17.6'W	2365 m	analysed to 12.62 m
SO35-180	North Fiji	14°20.5'S	177°00.2'E	2910 m	analysed to 5.50 m
SO35-182	North Fiji	14°30.2'S	177°05.6'E	3010 m	analysed to 0.69 m
SO35-211	North Fiji	14°23.2'S	177°08.7'E	2890 m	pilot core, to 0.67 m
SO35-272	North Fiji	16°01.2'S	177°41.4'E	3410 m	analysed to 8.24 m

Table 2.

a) Stable isotope data of *G. ruber* for core no. SO 35-101
(composite of the 315-400 μm and 250-315 μm size fractions)

Depth m	$\delta^{18}\text{O}$ ‰ vs PDB	$\delta^{13}\text{C}$ ‰ vs PDB	Depth m	$\delta^{18}\text{O}$ ‰ vs PDB	$\delta^{13}\text{C}$ ‰ vs PDB	Depth m	$\delta^{18}\text{O}$ ‰ vs PDB	$\delta^{13}\text{C}$ ‰ vs PDB
0.006	-1.29	0.69	0.406	-0.50	0.78	3.615	-0.90	0.26
0.011	-1.13	0.16	0.411	-0.55	0.62	3.765	-1.27	-1.75*
0.021	-1.25	1.16	0.436	-0.46	1.04	3.915	-0.63	-0.35
0.026	-1.09	1.00	0.431	-0.53	0.42	4.015	-0.53	-0.34
0.041	-1.23	0.92	0.446	-0.62	0.82	4.115	-0.60	-0.27
0.046	-1.37	0.57	0.451	-0.57	0.69	4.195	-0.61	-0.24
0.056	-1.29	0.73	0.508	-0.63	0.60	4.315	-0.58	0.24
0.061	-1.40	0.64	0.558	-0.64	0.72	4.385	-0.32	0.22
0.071	-1.61	0.46	0.608	-0.66	0.72	4.485	-0.52	-0.45*
0.076	-1.50	0.59	0.658	-0.61	0.72	4.585	-1.03	-0.02
0.086	-1.22	0.72	0.708	-0.72	0.50	4.715	-0.64	-0.17*
0.091	-1.30	0.55	0.758	-0.75	0.43	4.815	-0.91	-0.35*
0.106	-1.02	0.73	0.808	-0.67	0.68	4.915	-0.51	-0.90*
0.126	-0.92	0.29	0.848	-0.71	0.66	5.015	-0.57	0.08*
0.131	-0.67	0.26	0.908	-0.77	-0.28	5.145	-0.66	0.09
0.146	-0.46	0.80	0.958	-0.73	0.14	5.285	-0.39	0.42
0.151	-0.49	0.41	1.008	-0.76	0.21	5.415	-0.12	0.24
0.166	-0.30	0.74	1.165	-0.59	0.29	5.715	-0.57	0.61
0.171	-0.36	0.49	1.315	-0.78	0.41	5.815	-0.35	0.76
0.186	-0.37	0.63	1.465	-1.06	0.73	6.085	-0.04	0.23*
0.191	-0.23	0.58	1.585	-0.61	0.35*	6.495	-0.23	0.05*
0.206	-0.26	0.74	1.715	-1.17	0.41	6.765	-0.52	0.96
0.211	-0.17	0.61	1.915	-1.02	-0.49*	6.915	-0.89	0.70
0.226	-0.29	0.68	1.965	-0.70	-0.37	7.015	-0.45	-0.17
0.246	-0.17	0.80	2.075	-0.65	-0.21	7.165	-0.01	0.66
0.251	-0.06	1.18	2.215	-0.14	0.02	7.285	-0.04	-0.08*
0.266	-0.29	0.97	2.415	-0.57	0.24	7.415	-0.65	0.86
0.291	-0.19	0.71	2.545	-0.24	0.36	7.615	-0.33	0.03*
0.311	-0.30	0.54	2.625	-0.49	0.12	7.715	-0.21	0.10*
0.326	-0.27	0.55	2.715	-0.78	-0.05	7.865	-0.72	-1.18*
0.331	-0.54	0.59	2.885	-0.40	0.58	8.015	-0.48	-0.15
0.346	-0.49	0.52	3.015	-0.81	0.04*	8.115	-0.61	-0.93*
0.351	-0.11	1.22	3.115	-0.77	0.50	8.215	-0.61	0.98
0.368	-0.37	0.80	3.215	-1.33	0.01	8.315	-0.83	0.46
0.371	-0.48	0.76	3.315	-1.20	-0.37*	8.505	-0.87	0.49
0.386	-0.56	0.77	3.395	-1.12	0.03	8.615	-0.83	0.65
0.391	-0.57	0.52	3.515	-0.52	0.21	8.745	-0.83	0.55
Stable isotope data of <i>G. conglobatus</i> , 400-500 μm size fraction.								
6.915	-0.27	1.31	6.495	-0.39	1.69	6.085	-0.05	1.74
6.765	-0.30	1.32	6.365	-0.12	1.52	5.955	0.33	1.44
6.615	0.28	1.14	6.235	-0.26	1.18	5.815	0.28	1.37

* 250-315 μm size fraction only

Table 2.
b) Stable isotope data of *G. ruber* for core no. SO 35-117

Depth m	$\delta^{18}\text{O}$ ‰ vs PDB	$\delta^{13}\text{C}$ ‰ vs PDB	Depth m	$\delta^{18}\text{O}$ ‰ vs PDB	$\delta^{13}\text{C}$ ‰ vs PDB	Depth m	$\delta^{18}\text{O}$ ‰ vs PDB	$\delta^{13}\text{C}$ ‰ vs PDB
0.020	-1.51	0.11	4.520	-1.44	0.56	8.872	-1.08	-0.21
0.253	-1.01	0.16	4.653	-0.89	-0.53	9.020	-1.18	-0.48
0.408	-0.88	0.27	4.820	-0.91	0.15	9.067	-1.13	0.02
0.563	-0.91	-0.11	4.868	-0.43	-0.36	9.212	-0.18	-0.43
0.737	-0.68	-0.18	5.020	-0.78	-0.30	9.393	-0.56	0.07
0.820	-0.90	0.30	5.072	-0.37	0.03	9.520	-0.50	-0.62
0.913	-0.88	0.36	5.258	-0.17	0.46	9.572	-0.61	-0.78
1.020	-1.35	0.27	5.442	-0.64	0.21	9.772	-1.30	-0.17
1.063	-1.17	-0.16	5.520	-1.07	-0.08	9.820	-1.17	-1.14
1.243	-1.21	0.10	5.583	-1.10	-0.11	9.962	-1.36	-0.61
1.433	-1.23	0.05	5.753	-0.98	-0.04	10.020	-1.54	-0.69
1.520	-1.42	-0.24	5.820	-1.26	-0.69	10.163	-1.73	-0.56
1.638	-1.15	-0.46	5.923	-1.15	0.48	10.343	-0.96	-0.29
1.763	-0.34	-0.71	6.020	-1.72	-0.11	10.563	-0.75	-0.69
1.820	-0.46	-0.04	6.093	-1.54	0.29	10.620	-0.68	-1.00
1.933	-0.36	-0.26	6.248	-1.08	-0.21	10.743	-1.06	-1.13
2.020	-0.43	-0.23	6.422	0.18	-0.63	10.820	-1.06	-0.38
2.113	-0.40	0.00	6.520	-0.09	0.30	10.923	-1.14	-0.17
2.258	-0.66	-0.17	6.578	0.20	0.12	11.020	-1.36	-0.82
2.433	-0.63	-0.31	6.753	-0.49	-0.18	11.088	-0.58	-0.51
2.520	-0.90	0.10	6.820	-0.54	-0.27	11.263	-0.97	-0.33
2.633	-1.31	-0.36	6.953	-0.67	0.01	11.443	-1.12	-0.48
2.763	-1.23	-0.07	7.020	-0.66	-0.40	11.520	-1.42	-0.74
2.820	-1.11	-0.03	7.157	-0.53	-0.54	11.643	-1.38	-0.57
2.923	-1.14	-0.36	7.362	-1.17	0.14	11.820	-1.09	-0.65
3.020	-1.29	-0.73	7.520	-0.99	0.26	11.843	-0.88	-0.52
3.133	-1.05	-0.87	7.578	-0.99	0.67	12.020	-0.82	-0.48
3.292	-2.28	-0.93	7.752	-0.62	0.43	12.063	-0.50	-0.54
3.463	-1.34	-1.15	7.820	-0.80	0.43	12.238	-0.75	-0.95
3.520	-0.62	-0.50	7.923	-0.88	-0.09	12.413	-0.67	-0.60
3.653	-0.64	-0.13	8.020	-0.77	-0.36	12.573	-0.67	-0.14
3.753	-0.40	-0.15	8.087	-0.68	-0.59	12.620	-1.25	-0.63
3.820	-0.48	-0.07	8.270	-0.51	0.08	12.753	-1.02	-0.36
3.923	-0.56	0.01	8.272	-0.66	0.08	12.923	-1.20	0.08
4.020	-0.86	0.16	8.462	-1.11	-0.06	13.128	-0.80	-0.04
4.123	-0.52	0.60	8.520	-1.23	-0.51	13.160	-0.99	-0.46
4.277	-0.76	-0.15	8.672	-1.38	-1.03			
4.463	-1.25	-0.41	8.813	-0.78	-0.53			

Table 2.

c) Stable isotope data of *G. ruber* for core no. SO 35-119

Depth m	$\delta^{18}\text{O}$ ‰ vs PDB	$\delta^{13}\text{C}$ ‰ vs PDB	Depth m	$\delta^{18}\text{O}$ ‰ vs PDB	$\delta^{13}\text{C}$ ‰ vs PDB	Depth m	$\delta^{18}\text{O}$ ‰ vs PDB	$\delta^{13}\text{C}$ ‰ vs PDB
0.08	-1.19	0.68	4.40	-0.51	0.10	8.36	-0.50	-0.09
0.20	-0.70	0.91	4.50	-0.34	0.25	8.45	-0.29	-0.19
0.30	-0.50	0.34	4.65	-0.79	0.13	8.55	-0.44	0.06
0.45	-0.95	0.85	4.80	-0.82	0.75	8.66	-0.72	-0.50
0.55	-1.07	0.00	4.90	-1.00	0.01	8.77	-0.75	-0.26
0.70	-1.07	0.49	5.15	-0.95	0.20	8.88	-1.14	-0.34
0.85	-1.06	1.02	5.30	-0.99	0.46	8.99	-1.45	-0.44
1.00	-1.41	0.52	5.40	-1.61	0.63	9.15	-1.05	0.26
1.10	-1.61	0.22	5.45	-1.48	0.78	9.26	-0.88	0.42
1.20	-1.70	0.53	5.50	-1.76	0.52	9.55	-0.85	0.18
1.30	-1.27	0.78	5.55	-1.58	0.46	9.65	-0.90	0.00
1.40	-1.58	0.15	5.60	-1.63	0.26	9.75	-1.02	0.02
1.55	-0.62	0.26	5.64	-1.63	0.49	9.86	-1.35	0.02
1.70	-0.36	0.06	5.70	-1.34	0.34	9.98	-1.56	0.71
1.80	-0.51	-0.25	5.75	-1.32	0.45	10.10	-0.74	0.05
1.90	-0.58	0.26	5.85	-0.49	0.12	10.25	-0.48	0.45
2.00	-0.75	0.15	5.95	-0.29	0.28	10.35	-1.16	0.09
2.15	-1.00	-0.06	6.15	-0.59	0.18	10.48	-1.18	0.12
2.30	-1.15	0.36	6.25	-0.70	0.32	10.60	-1.20	-0.15
2.40	-1.26	0.19	6.35	-0.82	0.22	10.70	-1.40	-0.48
2.50	-1.18	0.18	6.45	-0.69	0.14	10.99	-1.25	0.04
2.70	-1.31	0.19	6.55	-0.55	0.74	11.10	-1.31	0.01
2.80	-1.03	-0.16	6.65	-1.19	0.53	11.45	-0.58	-0.37
3.00	-1.16	0.19	6.75	-1.31	0.91	11.55	-0.51	-0.25
3.15	-0.56	0.27	6.97	-1.05	0.60	11.65	-0.85	0.02
3.30	-0.30	-0.01	7.07	-1.23	1.03	11.75	-1.00	-0.73
3.40	-0.74	0.01	7.17	-1.03	0.71	11.92	-0.90	-0.24
3.50	-0.86	0.31	7.30	-0.86	0.66	12.02	-0.99	-0.17
3.65	-1.41	-0.04	7.43	-0.73	0.25	12.12	-1.13	0.20
3.80	-1.19	-0.05	7.60	-0.55	0.08	12.22	-1.30	0.55
3.90	-0.91	0.30	7.70	-0.82	0.22	12.32	-1.35	0.34
4.00	-1.16	0.22	7.80	-1.00	0.72	12.42	-1.31	0.29
4.15	-1.06	-0.15	8.00	-1.33	-0.40	12.52	-0.98	0.57
4.30	-1.48	-0.21	8.27	-1.07	0.12	12.62	-0.66	0.48

Table 2.

d) Stable isotope data of *G. ruber* for core no. SO 35-272

Depth m	$\delta^{18}\text{O}$ ‰ vs PDB	$\delta^{13}\text{C}$ ‰ vs PDB	Depth m	$\delta^{18}\text{O}$ ‰ vs PDB	$\delta^{13}\text{C}$ ‰ vs PDB	Depth m	$\delta^{18}\text{O}$ ‰ vs PDB	$\delta^{13}\text{C}$ ‰ vs PDB
0.042	-1.92	1.28	1.760	-1.40	1.22	3.920	-1.86	0.49
0.046	-1.97	1.21	1.800	-1.40	1.11	3.960	-1.76	1.09
0.081	-1.83	0.87	1.840	-1.69	1.00	4.000	-1.56	0.87
0.121	-1.61	0.68	1.880	-1.55	1.20	4.040	-1.65	1.31
0.141	-1.44	0.66	1.920	-1.88	0.61	4.080	-1.78	0.85
0.161	-1.42	0.37	1.960	-1.99	0.83	4.120	-1.87	0.77
0.171	-1.18	0.91	2.000	-1.34	1.36	4.160	-1.76	0.54
0.181	-0.84	0.99	2.040	-1.51	1.11	4.200	-1.87	0.26
0.191	-1.00	0.86	2.080	-1.66	0.73	4.240	-2.05	0.63
0.201	-0.73	1.14	2.120	-1.72	0.77	4.280	-2.11	0.19
0.211	-1.06	0.58	2.160	-1.44	1.28	4.320	-2.02	1.06
0.221	-0.69	0.29	2.200	-1.70	1.02	4.360	-2.09	0.62
0.231	-1.14	0.56	2.240	-1.89	0.41	4.400	-2.09	0.39
0.241	-1.17	0.52	2.280	-1.67	0.06	4.440	-2.12	-0.36
0.251	-1.08	0.90	2.316	-1.52	0.97	4.480	-1.78	0.17
0.261	-1.05	1.20	2.360	-1.69	0.58	4.600	-1.48	0.73
0.291	-0.84	1.29	2.400	-1.36	1.05	4.640	-2.30	-0.14
0.331	-0.81	1.29	2.440	-1.25	0.70	4.680	-2.34	0.73
0.360	-1.00	1.29	2.480	-1.28	1.20	4.720	-2.56	0.40
0.400	-0.92	1.23	2.520	-1.27	0.75	4.760	-2.82	0.10
0.440	-0.99	1.47	2.560	-1.43	0.87	4.800	-2.48	0.31
0.480	-1.09	1.19	2.600	-1.65	0.63	4.840	-2.31	0.54
0.520	-1.00	1.57	2.640	-1.16	0.21	4.880	-2.18	-0.02
0.600	-1.09	1.26	2.720	-1.45	0.98	4.920	-2.22	0.61
0.640	-1.25	1.01	2.760	-1.33	0.83	4.960	-2.36	0.42
0.680	-1.18	1.27	2.800	-1.33	0.15	5.000	-2.08	0.29
0.720	-1.26	0.99	2.840	-0.89	1.68	5.040	-2.04	0.30
0.760	-1.05	1.52	2.880	-0.91	0.59	5.080	-1.99	-0.04
0.800	-1.33	1.26	3.000	-1.25	1.22	5.090	-1.90	0.55
0.860	-1.22	1.27	3.040	-1.76	1.16	5.250	-0.86	0.33
0.920	-1.07	1.46	3.080	-1.38	0.75	5.360	-0.99	0.08
1.000	-1.33	0.91	3.120	-1.79	1.29	5.470	-0.90	0.79
1.080	-1.31	1.46	3.160	-1.57	1.27	5.600	-1.15	0.57
1.160	-1.52	0.94	3.200	-1.80	0.76	5.730	-1.01	1.01
1.200	-1.31	1.25	3.240	-1.84	1.10	5.850	-1.09	0.45
1.220	-1.28	0.87	3.280	-1.90	1.10	6.130	-1.13	0.62
1.240	-1.33	1.22	3.320	-1.86	1.22	6.250	-1.39	-0.11
1.260	-1.50	1.27	3.360	-2.07	1.37	6.350	-1.18	0.32
1.280	-1.28	1.43	3.400	-2.39	0.75	6.500	-1.54	0.31
1.300	-1.27	1.35	3.440	-2.06	0.41	6.650	-1.66	0.29
1.320	-1.36	1.27	3.480	-2.21	0.95	6.800	-1.58	0.39
1.360	-1.26	1.28	3.520	-2.13	1.10	6.900	-1.63	0.10

Table 2 d (continued)

Depth m	$\delta^{18}\text{O}$ ‰ vs PDB	$\delta^{13}\text{C}$ ‰ vs PDB	Depth m	$\delta^{18}\text{O}$ ‰ vs PDB	$\delta^{13}\text{C}$ ‰ vs PDB	Depth m	$\delta^{18}\text{O}$ ‰ vs PDB	$\delta^{13}\text{C}$ ‰ vs PDB
1.400	-1.44	1.38	3.560	-2.17	0.84	7.040	-1.11	0.85
1.440	-1.36	0.96	3.600	-1.68	0.97	7.170	-1.58	0.65
1.480	-1.86	0.82	3.640	-1.73	1.17	7.300	-1.93	0.40
1.520	-1.49	1.10	3.680	-1.86	1.21	7.450	-1.94	0.71
1.560	-1.43	0.75	3.720	-1.63	1.32	7.600	-1.82	0.59
1.600	-1.29	1.31	3.760	-1.74	0.87	7.750	-2.04	0.86
1.640	-1.49	1.22	3.800	-1.94	0.88	7.900	-1.80	0.32
1.680	-1.36	0.93	3.840	-1.77	0.79	8.060	-1.65	0.39
1.720	-1.53	0.76	3.880	-1.77	0.55	8.240	-1.48	0.60

Table 3. Oxygen isotope stratigraphy of the South Lau and North Fiji Basins.
Sedimentation rates (in parentheses) in cm/1000 yrs. apply to first named Isotope Stage.

Stage boundary	Age ka	South Lau Basin			North Fiji Basin		
		SO35-101 cm	SO35-117 cm	SO35-119 cm	SO35-182 cm	SO35-211 cm	SO35-272 cm
1/2	13.5	11.5 (1.2)		20 (1.7)	10 (1.8)	13 (1.3)	16 (1.6)
2/3	26.8	38 (2.1)		38 (1.4)	26 (1.2)	35 (1.7)	94 (5.9)
3/4	56.7	108 (2.3)					274 (6.0)
4/5	68.4	137 (2.5)	94				301 (2.3)
5/6	128.1	205 (1.1)	168 (1.3)	153 (1.1)			514 (3.6)
6/7	190.5	308 (1.7)	252 (1.8)	210 (0.9)			717 (3.3)
7/8	243.3	391 (1.6)	348 (1.9)	310 (1.9)			
8/9	301.0	451 (1.0)	430 (1.4)	350 (0.7)			
9/10	344.4	515 (1.5)	502 (1.7)	437 (2.0)			
10/11	377.1	600 (2.6)	545 (1.3)	480 (1.3)			
11/12	412.5	?700 (2.8)	634 (2.5)	582 (2.9)			
12/13	478.0	?780 (1.2)	720 (1.3)	660 (1.2)			
13/14	524.0		800 (1.7)	730 (1.5)			
14/15	565.0		840 (0.9)	775 (1.1)			
15/16	620.0		915 (1.4)	830 (1.0)			
16/17	659.0		966 (1.3)	875 (1.2)			
17/18	689.0		1027 (2.0)	924 (1.6)			
18/19	726.6		1086 (1.6)	980 (1.5)			
19/20	736.0		1105 (1.9)	1009 (2.9)			
20/21	763.0		1134 (1.1)	1030 (0.8)			
21/22	790.0		1194 (2.2)	1130 (3.7)			
22/23			1258	?1200			
23/24				1258			
Average sedi- mentation rates		1.7	1.5	1.4		4.6	5.7

Table 4. Samples of core no. SO 35—110, which are strongly affected by diagenetic alteration (selective dissolution)

Depth m	$\delta^{18}\text{O}$ (‰)	Estimated deviation in isotope value (‰)
1.09	0.20	1.0
2.12	1.02	0.6
3.62	2.05	1.2
3.88	1.25	0.4 (plotted)
5.25	1.58	0.7 (plotted)
5.37	2.14	1.4
7.37	2.27	1.5
7.50	2.20	1.5

Table 5. Organic carbon, carbonate and sulphur accumulation rates, and new paleoproductivities in the South Lau and North Fiji Basins ($\text{g}/\text{m}^2\text{a}$)

Core No. SONNE 35	Carbonate		Accumulation rates				Paleoproductivity Organic Carbon	
	(a)	(b)	Organic Carbon (a)	(b)	Sulphur (a)	(b)	(a)	(b)
—101	3.305	4.497	0.019	0.023	0.009	0.012	6.83	8.06
—102	5.446	—	0.009	—	—	—	3.01	—
—182	—	5.341	—	0.015	—	—	—	5.76
—211	5.985	6.794	0.005	0.004	—	—	2.68	3.04
—272	5.385	6.090	0.026	0.048	0.007	0.014	9.80	21.44

(a) 0—8,000 years B.P.

(b) 17,000—21,000 years B.P.